IEEE Access
Multidisciplinary | Rapid Review | Open Access Journal

Date of publication xxxx 00, 0000, date of current version xxxx 00, 0000.

Digital Object Identifier 10.1109/ACCESS.2017.Doi Number

Integrated Outage Management with Feeder Restoration for Distribution Systems with DERs

Chensen Qi[1], Student Member, IEEE, and Chen-Ching Liu[1], Life Fellow, IEEE

[1] ECE Department, Virginia Tech, VA 24061 USA

Corresponding author: Chensen Qi (e-mail: qcs@vt.edu).

This work was supported by the U.S. Department of Energy under AGGREGATE project DE-OE0000878 in collaboration with Washington State University

ABSTRACT The increasing deployment of distributed energy resources (DERs) and microgrids benefits power grids by improving system resilience. In a resilience mode without the utility system, the distribution grid relies on DERs to serve critical load. In such a severe event with multiple faults on the distribution feeders, actuation of various protective devices (PDs) divides the distribution system into electrical islands. The undetected actuated PDs due to fault current contributions from DERs can delay the restoration process, thereby reducing the system resilience. In this paper, algorithms are proposed for outage management and feeder restoration for distribution systems with multiple DERs. The Advanced Outage Management (AOM) identifies the faulted sections and actuated PDs in a distribution system with DERs by incorporating smart meter data. The Advanced Feeder Restoration (AFR) is proposed to restore a distribution system with available energy resources taking into consideration the availability of utility sources and DERs as well as the feeder configuration. By partitioning the system into islands, critical load will be served with the available generation resources within islands. When the utility systems become available, the optimal path will be determined to reconnect these islands back to substations and restore the remaining load. The proposed method has been validated with modified IEEE 123-Bus and 8500-Node Test Feeders. Simulation results demonstrate the capability of the integrated AOM and AFR to enhance distribution system resilience.

INDEX TERMS Outage Management, Feeder Restoration, Distributed Energy Resources, Distribution Systems, Resilience

I. INTRODUCTION

Resilience of a distribution system is its capability to withstand and recover rapidly from major disasters [1]. These extreme events are rare, but they can be catastrophic [2]. The resilience of a distribution system is quantified by the MWh capability to serve critical load over the specified service restoration period [1-3]. DERs within the scope of this study include distributed generators (DGs), batteries, and renewable energy integrated with storage devices that meet the requirements of IEEE 1547 standard [4]. The DERs with proper control capability [5] can support service restoration by providing electric energy to critical loads when utility sources are not available. However, DERs in a distribution system usually have relatively small generation capacity. Hence, it is beneficial to use multiple DERs, if available, to improve system resilience. To this end, two important issues arise: (1) how to optimally allocate and control multiple DERs to pick up and serve critical loads in electrical islands when the utility system is unavailable, and (2) when the utility sources become available, how to restore the remaining load efficiently. In [6-8], mixed integer linear programming methods are proposed to form islands for restoration of critical loads. The methods in [1, 9] provide restoration strategies to use microgrids to serve critical loads. In [10-12], system reconfiguration methods are proposed to serve loads with utility sources. In [13], a method is developed regarding allocation of mobile energy resources. However, there is not a systematic method to identify system restoration strategy using multiple DERs based on the available utility sources and system configuration.

As additional generation and load resources, DERs can also make system protection and control more complex. Conventionally, distribution systems are equipped with well-coordinated PDs for one-directional power flow based on the fault currents [14]. The increasing penetration of DERs increases the risk of protection miscoordination [15]. As a result, fault currents from DERs may actuate PDs that are not expected to operate [16].

With deployment of smart devices including smart meters as well as remote monitored fault indicators (FIs), the accuracy

This article has been accepted for publication in a future issue of this journal, but has not been fully edited. Content may change prior to final publication. Citation information: DOI 10.1109/ACCESS.2021.3103477, IEEE Access

and efficiency of outage management is enhanced. In [17-18], outage management methods with Automatic Meter Reading (AMR) are proposed. The technical challenges of outage management in distribution systems with high penetration of DERs can be summarized by: (1) meshed system, (2) unknown actuated PDs, and (3) incomplete and noisy information.

Due to limitations of communication systems, outage notifications from smart meters may be erroneous. FI reports can be missing or incorrect. Most existing fault diagnosis [19-21] methods require complete outage information. In the authors' prior work, a hypothesis-based method is proposed [22] to handle incomplete evidence by ranking the credibility of hypotheses. However, the method is only applicable to a radial distribution system without DERs. Existing outage management methods for meshed systems [19-21, 23] are not designed with the capability to identify PDs actuated by fault currents contributed by DERs.

In [24], smart meters are incorporated to identify the fault location based on evidence from the voltage sag reports. In [25], a method is proposed to identify high impedance faults in a distribution system with voltage data from smart meters. Both methods require synchronized smart meter data. However, due to limitations of the communication capability, under severe outage conditions, high latency and drop rate can be expected with a high-volume smart meter data being sent within a short period. In [26] the impact of a delay in smart meters data is analyzed. Furthermore, the clocks of smart meters are not GPS-synchronized. (For some types of smart meters, clock synchronization can be automatically triggered when the clock deviates within a predefined threshold [27].) In [28], the existence of nested outages due to actuation of unknown PDs and its impact to service restoration is discussed. However, to the best of the authors' knowledge, there is not a systematic method to identify those PDs that are actuated and the associated nested outages due to the lack of measurements. In this paper, an Advanced Outage Management with Feeder Restoration algorithm is proposed. Compared with the existing outage management methods, the contributions of the proposed AOM method are: (1) a hierarchical method is proposed to detect actuated PDs due to fault current contributions from DERs. Those unknown PDs are detected with smart meter event timestamps. (2) An integer linear programming for a meshed system model is proposed to incorporate hypotheses and incomplete evidence. The AOM is integrated with the Advanced Feeder Restoration (AFR) module that incorporates the effect of DERs in a distribution system. In comparison with existing restoration methods, the contributions of the proposed AFR are: (1) A distributed control structure is proposed for the islands. This structure can use small DERs to provide service to critical load. (2) The new method considers the control capabilities and availability of different types of energy resources. Note that the island boundary varies based on the availability of DERs and utility system. The proposed algorithm provides an optimal operation sequence for both DERs and switches to reconnect with the utility source when it becomes available.

The remaining of this paper is organized as follows. The problem formulation of the proposed AOM with AFR is given in section (II). The mathematical formulation of AOM method is described in section (III). The mathematical model of AFR is provided in section (IV). The test scenarios of IEEE 123-Bus and 8500-Node systems and their test results are included in section (V). The conclusion is given in section (VI).

II. INTEGRATED AOM WITH AFR

Upon occurrence of single- or multiple-faults, the appropriate PDs among substation breakers, reclosers, sectionalizers, and fuses will be actuated to isolate the fault(s) and minimize the load service disrupted by the event. Smart meters inside the isolated area detect the sustained power outage and send power outage notifications (PONs) with the event timestamps. However, due to the high-volume communication within a short period and possible malfunctioning of smart meters, outage notifications can be missing or delayed. Although some smart meters are equipped with automatic clock synchronization function, it is triggered only when the time deviation exceeds a predefined threshold. Therefore, the event timestamps recorded by the outage notifications during hazards can be erroneous. Remote-monitored FIs including Non-Directional FI, Uni-Directional FI, and Bi-Directional FI [20-21] are designed to send fault current reports. Since devices can malfunction and the underlying communication facilities can be damaged under a severe event, the FI reports can be missing or incorrect. In the distribution system with high penetration of DERs, as illustrated in Fig. 1, DERs with high capacity are equipped with PDs to provide anti-island capability under abnormal conditions to cut off the fault current contribution. However, due to possible prolonged DER fault current contributions from a corresponding PD failure or miscoordination of PDs, unexpected PDs in the distribution system can also be triggered. For the feeder with a permanent fault as shown in Fig. 1, fuse 7 (F7) may be melted by the fault current from the distributed generator DER2 before the reclosing process of R2 is completed.

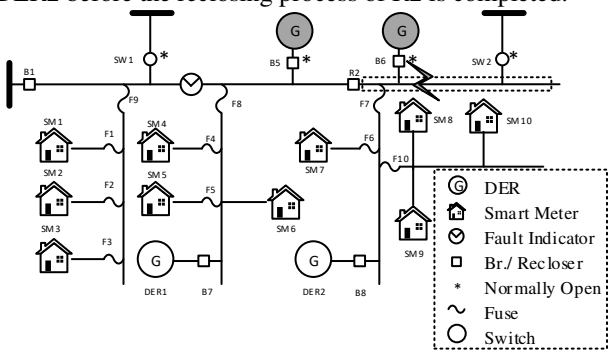

FIGURE 1. A distribution feeder with DERs

PDs will be actuated sequentially depending on their coordination. Therefore, the event timestamps of outage notifications serve as evidence of the PD actuations. In this

This article has been accepted for publication in a future issue of this journal, but has not been fully edited. Content may change prior to final publication. Citation information: DOI 10.1109/ACCESS.2021.3103477, IEEE Access

paper, the proposed AOM is a hypothesis-based hierarchical method. To handle the incorrect or missing outage notifications by smart meters, a list of hypotheses is generated. These hypotheses include the number of faults N_{fault} for the first level. It identifies the outage area(s) based on outage notifications from smart meters. Since the power outage follows the actuation of PDs upon the occurrence of faults, the boundary of an outage area is the PD that interrupts the fault current from the substation. The PD with the maximum number of PONs downstream from the substation is the boundary point.

In each outage area determined at the first level, the second level outage management will be applied to handle the errors of event timestamps associated with outage notifications of smart meters and missing/error reports of FIs. The second level hypotheses include the number of mis-coordinated PD pairs between DERs and the distribution system $N_{DER.mis}$, number of miscoordinated PD pairs in the distribution system $N_{Prot.mis}$, and number of FI failures $N_{FI.failure}$. The actuated PD(s) in an outage area will divide the outage area into multiple outage blocks. The number of outage blocks N_{block} is equal to the number of actuated PD(s) in this area. Except for the boundary PD which is opened due to the fault current from the substation, an actuated PD in this outage area corresponds to a mis-coordinated pair between a DER and another PD. The numerical relationship between N_{block} and $N_{DER.mis}$ is given by

$$N_{block} = N_{DER.mis} + 1 \quad (1)$$

Although $N_{DER.mis}$ is given by the hypothesis, it is also constrained by the inequality of

$$N_{DER.mis} \leq N_{DER} \quad (2)$$

where N_{DER} is the number of DERs in this outage area.

Fig. 2 illustrates the relationship among the outage area, outage block, and PD actuations. The outage area indicated by the dashed line in Fig. 2 (a) contains 3 outage blocks represented by the gray areas in Figs. 2 (b), (c), and (d). PDs 1, 2, 3, 4, and 5 are located inside the outage area, where the actuated PD 1 is identified as the boundary. The outage block indicated in Fig. 2 (b), is surrounded by multiple actuated PDs. The actuated PD 1 is the PD closest to the substation which is defined as upstream actuated PD. The other actuated PDs 3 and 4 which are further away from the substation are called downstream actuated PDs. Due to the radial structure of the distribution system regardless of DERs, each outage block will have one PD and all the other actuated devices surrounding this block are downstream actuated PDs. Note that PDs inside the outage area may not be actuated. In Fig. 2 (b), PDs 3 and 4 are downstream the actuated PDs of this outage block. PD 2 lies inside this outage block. The downstream actuated PD of an outage block is also the upstream actuated PD of another outage block, as illustrated in Figs. 2 (b) and (c). PD 3 is a downstream PD of the outage block as shown in Fig. 2 (b). It is also the upstream actuated PD of the outage block in Fig. 2 (c).

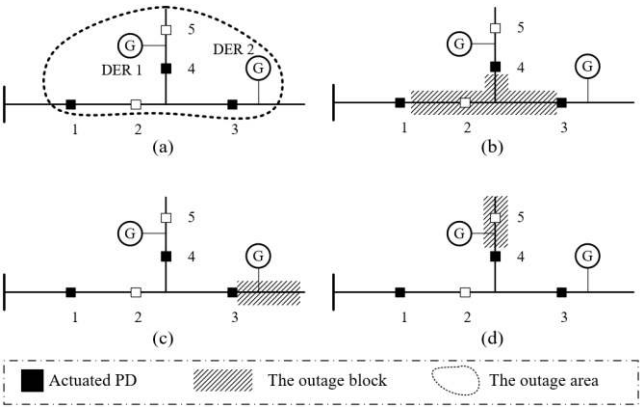

FIGURE 2. Actuated PDs surrounding an outage block

In an extreme event with multiple faults, DERs and microgrids are used to pick up and serve the critical loads. However, DERs are usually limited in capacity. Coordinating multiple DERs to form islands and regulate the frequency and voltage is essential to provide reliable service.

The AFR algorithm has two levels. The first level determines the system reconfiguration strategy to establish a sequence of topologies for service restoration process. In this level, the availability of utility sources is incorporated to minimize the restoration period. Changing the topologies requires synchronization of islands. The second level provides operations of DERs and microgrids based on the availability of different energy resources to restore load.

Data transfer between the Advanced Distribution Management System (ADMS) and the proposed methods is illustrated in Fig. 3. During a normal situation, AOM and AFR modules keep track of the system topological changes due to operations. In an extreme event, upon receiving the PONs and fault current reports via Meter Data Management System (MDMS) and Supervisory Control And Data Acquisition system (SCADA), the fault location(s) and PD actuation(s) will be identified by the AOM. While waiting for the outage scenario that is identified, AFR collects the controllability information of DERs and microgrids via DER Management System (DERMS) and Microgrid Management System (MGMS). Data transfer between AOM and AFR is represented by the box on the left side of Fig. 3. The identified outage scenario of AOM will be checked by the system operator. The validated outage scenario incorporating fault locations and actuated PDs will be sent to AFR. Based on the outage scenario identified, an optimal restoration path is determined by the first level AFR to reconnect outage islands to the utility source once it becomes available. The second level AFR will be applied to the topology determined in the first level to determine DER and switching operations. The proposed optimal restoration strategy will be validated by power flow computation. The corresponding feasible control strategy will be applied via DERMS and MGMS.

This article has been accepted for publication in a future issue of this journal, but has not been fully edited. Content may change prior to final publication. Citation information: DOI 10.1109/ACCESS.2021.3103477, IEEE Access

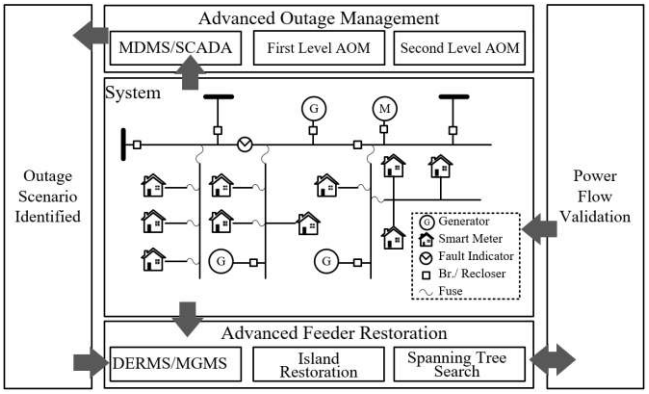

FIGURE 3. Schematic diagram and data transfer

The proposed AOM and AFR will only require data or notifications collected within a specified rolling time window, e.g., 1 minute after receiving the last PON, to determine the outage scenario and the optimal restoration strategy. Based on the simulation results, the performance of AOM/AFR is not sensitive to the number of faults in the system. However, it is sensitive to the scale of the system and number of timesteps in the restoration process.

III. ADVANCED OUTAGE MANAGEMENT (AOM)

A. First Level Outage Management

After the actuation of PD (s) to isolate fault (s), smart meters will send PONs to report sustainable power outage events that last longer than a predefined period T_{PON}, say, 45 seconds. The proposed AOM module will be triggered by the first PON received and collect PONs until $t_{last} + T_{PON}$ plus a threshold, say 15 seconds, where t_{last} is the time when the last PON is received by AOM. The objective of this level is to identify those outage areas in the distribution system after receiving PONs from smart meters.

1) Objective function: The proposed AOM identifies actuated PD and fault locations based on the outage event timestamps recorded in PONs from smart meters. However, the timestamps of different faults in the system depend on the sequence of faults. To handle multiple fault scenarios, the first level AOM is applied to identify the outage area associated with each fault. In this level, a list of hypotheses will be generated automatically including the number of faults N_{fault}. The maximum possible number of faults can be determined by the experience of the operator. In each hypothesis, an outage area is associated with a fault. The objective of this level is described by the following objective function,

$$Max \sum_{k\in\Omega_{Fault}} \sum_{i\in\Omega_{Prot}} y_i^k \left(SM_i + \frac{1}{M} Level_i\right) \quad (3)$$

where y_i^k is the binary decision variable. If PD i is the boundary of the outage area associated with fault k, it will be 1; otherwise, it will be 0. Ω_{Fault} is the set of faults. Ω_{Prot} is the set of PDs. SM_i is the parameter representing the number of PONs downstream PD i from the substation. This parameter is given by the power outage notifications received from smart meters upon the occurrence of a fault. $Level_i$ is the parameter which is the number of PDs between PD i and the substation, a parameter given by the system topology. It represents the distance between PD i and the substation. By selecting a proper value for parameter M, for each fault k, the algorithm finds the farthest PD from the substation with the maximum number of PONs downstream. One of the M values can be selected as $N_{Fault} * N_{Prot}$. N_{Prot} is the number of PDs in this system. The number of faults, N_{Fault}, is specified for each hypothesis and the credibility of each hypothesis is then evaluated based on the evidence available.

2) Constraints: As mentioned previously, there is an outage area that corresponds to each fault for a given hypothesis. This constraint is described by an equality constraint, i.e.,

$$\sum_{i\in\Omega_{Prot}} y_i^k = 1, \forall k \in \Omega_{Fault} \quad (4)$$

$$\sum_{k\in\Omega_{Fault}} \sum_{j\in\Omega_{Prot.UP.i}} \left(y_j^k + y_i^k\right) \le 1, \forall\, i \in \Omega_{Prot} \quad (5)$$

where $\Omega_{Prot.UP.i}$ is the set of PDs upstream PD i from the substation. Constraint (5) indicates that one outage area does not overlap another outage area.

The first level outage management is a binary integer programming (IP) which is solved efficiently by off the shelf software. For instance, one hypothesis for the first level AOM of IEEE 123-Bus system is calculated in about 1 second using the Gurobi solver.

B. Second Level Outage Management

The event timestamps are recorded in the PONs sent from smart meters which represent the actuation of corresponding PDs. Therefore, the PD actuations as well as the fault location can be determined based on these event timestamps. In each outage area determined at the first level, the second level AOM is applied. The objective of this level is to identify the fault location, PD mis-coordination, and FI failures in the outage area associated with each fault.

To determine the actuated PD(s) and the fault location in this outage area, the notifications that are caused by other faults should be removed by taking the following steps:

(1) Remove the PONs from smart meters outside the outage area, (2) Remove the FI reports from the branch that is adjacent with another outage area.

By removing PONs associated with the other faults in the system, timestamps recorded in the PONs follow the coordinated settings of PDs due to the fault contained in this outage area. PONs in one outage block associated with the same actuated PD in this outage area will have similar timestamps. To identify these similarities, PONs from smart meters in the outage area will be clustered into N_{block} clusters based on the timestamps of PONs. N_{block} is given by (1).

The cluster algorithm has an objective function of

$$Min \sum_{i=1}^{N_{block}} \sum_{j\in\Omega_{SM.PON.area}} \left\|T_j - \mu_i\right\|^2 \quad (6)$$

This article has been accepted for publication in a future issue of this journal, but has not been fully edited. Content may change prior to final publication. Citation information: DOI 10.1109/ACCESS.2021.3103477, IEEE Access

where T_j represents the event timestamp of the PON from smart meter j, and μ_i is the average event timestamp of cluster i. $\Omega_{\text{SM.PON.area}}$ is the set of smart meters in this outage area that send PONs for this outage event. The objective function (6) can be calculated by the K-means clustering algorithm.

Ideally, if timestamps accurately represent the PD actuations for the fault in this outage area, the clusters identified in (6) will be able to represent outage blocks divided by actuated PDs. However, since smart meter clocks generally are not GPS-synchronized, the event timestamps recorded in PONs can be erroneous and may not be able to represent correct timing of the outage event. To identify the most credible outage scenario, an optimization problem is solved incorporating system topologies after the clustering process.

3) Objective function: Since clusters may not accurately represent outage blocks, an integer linear programming problem is solved to determine the most credible scenario for this hypothesis. The objective is to determine the group of PDs corresponding to the maximum number of PONs in the corresponding cluster. It is described by an objective function, i.e.,

$$Max \sum_{k\in\Omega_{Block}} \sum_{i\in\Omega_{Prot}} u_i^k SM_{i.Prot}^k + \left(\frac{v_i^k}{2M_1} - \frac{h_i^k}{2M_2}\right) Level_i \quad (7)$$

where $\Omega_{Block}$is the set of outage blocks clustered in (6). $SM_{i.Prot}^k$ is the parameter representing the number of PONs downstream PD i from the substation clustered in the block k by (6) . u_i^k is an integer variable. v_i^k , and h_i^k are binary variables. If PD i is the upstream actuated PD in outage block k , u_i^k will be 1. If PD i is the downstream actuated PD in outage block k, u_i^k will be -1. Otherwise, u_i^k will be 0. On the other hand, if PD i is the upstream actuated PD in outage block k , v_i^k will be 1, while if PD i is the downstream actuated PD in outage block k , h_i^k will be 1. In other cases, they will be 0. The parameter M_1 and M_2 are two large numbers. In this algorithm, they can be selected as $N_{block} * N_{Prot}$and $N_{block} * (N_{Prot})^2$ where the number of blocks, N_{block}, is given by each hypothesis.

The actuation of PDs, outage blocks, FI failures and fault location for this outage area are determined with several constraints:

4) Topology constraints: The outage block topology constraints need to be represented. Note that on each path, an outage block can have at most two actuated PDs. That is,

$$h_i^k \le b_i^k, \forall k \in \Omega_{Block}, i \in \Omega_{Prot} \quad (8)$$

$$h_i^k \le z_i^k, \forall k \in \Omega_{Block}, i \in \Omega_{Prot} \quad (9)$$

$$h_i^k \ge b_i^k + z_i^k - 1, \forall k \in \Omega_{Block}, i \in \Omega_{Prot} \quad (10)$$

$$u_i^k + \sum_{j\in\Omega_{Prot.UP/i}} u_j^k \ge 0, \forall k \in \Omega_{Block}, i \in \Omega_{Prot} \quad (11)$$

$$b_i^k = \sum_{j\in\Omega_{Prot.UP/i}} u_j^k, \forall k \in \Omega_{Block}, i \in \Omega_{Prot} \quad (12)$$

$$u_i^k = -2h_i^k + z_i^k, \forall k \in \Omega_{Block}, i \in \Omega_{Prot} \quad (13)$$

$$v_i^k \le -h_i^k + z_i^k, \forall k \in \Omega_{Block}, i \in \Omega_{Prot} \quad (14)$$

$$v_i^k \ge z_i^k, \forall k \in \Omega_{Block}, i \in \Omega_{Prot} \quad (15)$$

where b_i^k, z_i^k are binary variables. b_i^k will be 1 if PD i is inside the outage block k or the downstream actuated PD of the outage block k. z_i^k will be 1 if PD i is actuated in outage block k . Otherwise, they will be 0. $\Omega_{Prot.UP/i}$ is $\Omega_{Prot.UP.i}$ excluding PD i. Constraints (8)-(15) indicate that, if there are two actuated PDs on each path, the one upstream will be the upstream actuated PD, and the downstream PD will be downstream actuated PD. This relationship is illustrated in Fig. 2 (b) where actuated PDs 1 and 3 are on one path, while actuated PDs 1 and 4 are on another path through the outage block. Among these PDs, actuated PD 1 is the upstream actuated PD while PD 3, and 4 are downstream actuated PDs. Constraints (8)-(10) are the linear relaxation of $h_i^k = b_i^k * z_i^k$ with *McCormick Envelopes* [29]. Since h_i^k, b_i^k, z_i^k are binary variables, linear relaxation can accurately represent this equation. Constraints (11)-(15) indicate that, on each path, there exists at least one upstream actuated PD for each block. This relationship is shown in Figs. 2 (c) and (d) where actuated PDs 3 and 4 are upstream actuated PDs for each outage block, respectively.

The topology relationship between two different outage blocks is constrained by

$$v_i^k \le 1 - b_i^j + h_i^j, \forall k, j \in \Omega_{Block}, i \in \Omega_{Prot} \quad (16)$$

$$\sum_{k\in\Omega_{Block}} v_i^k \le 1, \forall i \in \Omega_{Prot}, \quad (17)$$

$$C \sum_{k\in\Omega_{Block}} v_i^k \ge \sum_{k\in\Omega_{Block}} h_i^k, \forall i \in \Omega_{Prot} \quad (18)$$

$$u_i^k \ge Flag_i, \forall k \in \Omega_{Block}, i \in \Omega_{Prot} \quad (19)$$

$$\sum_{i\in\Omega_{Prot}} v_i^k = 1, \forall k \in \Omega_{Block}, \quad (20)$$

where $Flag_i$ is a parameter. It is -1 if there is any energy source connecting downstream PD i that can contribute fault current and cause PD miscoordination. Otherwise, it is 0. C can be any constant larger than N_{Block} in this hypothesis. Constraint (16) indicates that an upstream actuated PD of an outage block should not be inside another outage block. Constraint (17) ensures that a PD can be upstream actuated PD only once. Constraint (18) guarantees that a downstream actuated PD of an outage block will also become the upstream actuated PD of another outage block. This relationship is shown in Figs. 2 (b), (c), and (d). The downstream actuated PDs 3 and 4 in (b) are upstream actuated PDs in (c) and (d), respectively. Constraint (19) indicates that only the PDs with DERs connected downstream can become a downstream actuated PD. Constraint (20) means that an outage block will have one upstream actuated PD.

5) PD actuation constraints: These constraints guarantee that the outage blocks are surrounded only by those PDs that can be actuated due to the fault. As illustrated in Fig. 2 (a), the

This article has been accepted for publication in a future issue of this journal, but has not been fully edited. Content may change prior to final publication. Citation information: DOI 10.1109/ACCESS.2021.3103477, IEEE Access

fault current contributed by 1 DER can actuate at most 1 PD. In this scenario, PD 3 and PD 4 are actuated by the fault currents from DER 2 and DER 1, respectively. PD 1 is actuated by the fault current from the substation. The constraints are

$$\sum_{i\in\Omega_{Section}} F_i = 1 \quad (21)$$

$$z_i^k \le f_i \le \sum_{k\in\Omega_{Block}} z_i^k, \forall k \in \Omega_{Block}, i \in \Omega_{Prot} \quad (22)$$

$$1 - e_i^p \ge f_{\Omega_{Prot.p.Up/i}}, \forall p \in \Omega_{ERs}, i \in \Omega_{Prot} \quad (23)$$

$$1 - e_i^p \le \sum_{j\in\Omega_{Prot.p.Up/i}} f_j, \forall p \in \Omega_{ERs}, i \in \Omega_{Prot} \quad (24)$$

$$f_i \le \sum_{p\in\Omega_{ERs}} e_i^p, \forall i \in \Omega_{Prot} \quad (25)$$

$$\sum_{j\in\Omega_{Section.p.Down.i}} F_j = g_i^p, \forall k \in \Omega_{Block}, p \in \Omega_{ERs}, i \in \Omega_{Prot} \quad (26)$$

$$f_i \le \sum_{p\in\Omega_{ERs}} g_i^p, \forall i \in \Omega_{Prot} \quad (27)$$

$$N_{Prot.mis}, = \sum_{i\in\Omega_{Prot}} \sum_{p\in\Omega_{ERs}} g_i^p - e_i^p \quad (28)$$

where F_i, f_i, e_i^p, g_i^p are binary variables. F_i is 1 if section i contains the fault. If PD i is actuated, f_i will be 1; otherwise, it will be 0. e_i^p will be 0 if PD i is downstream another actuated PD with respect to energy resource p; otherwise, it will be 1. When PD i is upstream the fault with respect to energy resource p, g_i^p will be 1; otherwise, it will be 0. Ω_{ERs} is the set of energy resources. $\Omega_{Prot.p.Up/i}$ is the Ω_{Prot} upstream PD i from energy resource p excluding PD i. $\Omega_{Section}$ is the set of line sections. $\Omega_{Section.p.Down.i}$ is the $\Omega_{Section}$ downstream PD i from energy resource p. Constraint (21) indicates that there is one fault in each outage area. Constraint (22) stores all the actuated PDs in one vector. Constraints (23)-(25) indicate that a fault current due to one energy resource will be interrupted by only one PD. Constraints (26)-(27) indicate that the actuated PD is upstream the fault with respect to an energy resource. Constraint (28) is the hypothesis constraint of $N_{Prot.mis}$.

6) FI status constraints: The following constraints describe malfunctions of FIs in one outage area.

$$l_{down.i} = \sum_{k\in\Omega_{Section.Down.FI.i}} F_k, \forall i \in \Omega_{FI} \quad (29)$$

$$l_{up.i} = \sum_{k\in\Omega_{Section.Up.FI.i}} F_k, \forall i \in \Omega_{FI} \quad (30)$$

$$-h.FI_{up.i} \le FI_{up.i} - l_{up.i} \le h.FI_{up.i}, \forall i \in \Omega_{FI} \quad (31)$$

$$h.FI_{up.i} \le 2 - FI_{up.i} - l_{up.i}, \forall i \in \Omega_{FI} \quad (32)$$

$$h.FI_{up.i} - FI_{up.i} \le l_{up.i}, \forall i \in \Omega_{FI} \quad (33)$$

$$-h.FI_{down.i} \le FI_{down.i} - l_{down.i} \le h.FI_{down.i}, \forall i \in \Omega_{FI} \quad (34)$$

$$h.FI_{down.i} \le 2 - FI_{down.i} - l_{down.i}, \forall i \in \Omega_{FI} \quad (35)$$

$$h.FI_{down.i} - FI_{down.i} \le l_{down.i}, \forall i \in \Omega_{FI} \quad (36)$$

where $l_{down.i}$ and $l_{up.i}$ are two binary variables. Constraints (29) and (30) indicate that, if the fault is downstream (upstream) the FI i, $l_{down.i}$ ($l_{up.i}$) will be 1; otherwise, they will be 0. $\Omega_{Section.Up.FI.i}$ ($\Omega_{Section.Down.FI.i}$) is the $\Omega_{Section}$ upstream (downstream) FI i from the substation. $FI_{down.i}$ ($FI_{up.i}$) is the parameter of fault and FI relationship based on the received fault current report, respectively. Ω_{FI} is the set of FIs in this outage area. Constraints (31)-(36) indicate that if the FI status received is different from the value calculated, the corresponding binary variable $h.FI_{up.i}$ ($h.FI_{down.i}$) will be 1; otherwise, it is 0.

Constraints are formulated to incorporate the FI failure (s), i.e.,

$$FI.error_i \ge h.FI_{up.i}, \forall i \in \Omega_{FI} \quad (37)$$

$$FI.error_i \ge h.FI_{down.i}, \forall i \in \Omega_{FI} \quad (38)$$

$$FI.error_i \le h.FI_{down.i} + h.FI_{up.i}, \forall i \in \Omega_{FI} \quad (39)$$

$$N_{FI.failue} = \sum_{i\in\Omega_{FI}} FI.error_i \quad (40)$$

where $FI.error_i$ is to indicate the malfunction of FI i. If the FI i fails, it will be 1; otherwise, it will be 0. Constraints (37)-(39) model the bi-directional FI. These three constraints can be modified based on FIs' capabilities to indicate fault current directions. Constraint (40) is the hypothesis constraint of $N_{FI.failue}$.

In a large system, multiple faults can be associated with one outage area. In the outage scenario indicated by Fig. 4, the actuation status of PD 2 surrounded by multiple faults will depend on the sequence of the faults in this system. Since the smart meter clocks are not GPS-synchronized, the sequence of faults indicated by the outage notification timestamps from smart meter is not known accurately. Therefore, the proposed AOM will not be able to identify the actuation of PD indicated by the gray box in this figure. To handle this situation, the proposed AOM can be extended by including another level hypotheses incorporating the sequences of faults in the system. However, the calculation with this extension will be more complicated compared to the proposed AOM.

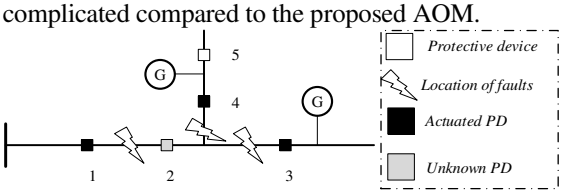

FIGURE 4. Multiple faults isolated in one outage area without DERs in the middle

In the future, the fault diagnosis method in [21] can be applied to estimate the locations of faults in this system with FI reports. By applying the proposed AOM into small islands where the assumption that each outage area contains one fault is valid based on the estimated fault locations, the most credible outage scenario can be identified for the given scenario in Fig. 4. As more sensors become available in the smart distribution system, future work is needed to identify the accurate fault locations without the need of this assumption.

This article has been accepted for publication in a future issue of this journal, but has not been fully edited. Content may change prior to final publication. Citation information: DOI 10.1109/ACCESS.2021.3103477, IEEE Access

As a hypothesis-based method, the performance of the second level AOM depends on the hypothesis of the first level AOM. By the proposed method, the results that match the outage evidence received in the first level will be given a higher credibility index and identified as the credible outage scenario. However, correct identification of the fault locations and PD actuations depends on the hypothesis of the first level AOM. The effect of the first level hypothesis to the second level falls into one of the two following cases:

(1) The number of faults in the hypothesis is larger than the number of faults in the system:

In this scenario, some outage area(s) identified in the first level will not contain any fault. If the second level AOM is applied to those outage areas that do not contain any fault, the PD actuations and fault locations identified in this scenario will not be meaningful.

(2) The number of faults in the hypothesis is smaller than the number of faults in the system:

In this scenario, some outage areas identified in the first level will contain multiple faults.

The effect on the second level AOM depends on the sequence of faults. If multiple faults occur within the same short time period, the timestamps of PONs associated with the outage blocks for each fault will not be distinguished by the proposed AOM. In this case, the actuated PDs and outage blocks may be incorrectly identified by AOM.

C. Credibility Evaluation

Credibility is a measure of the gap between the scenarios defined by each hypothesis (SDH) and the corresponding evidence received. Higher credibility means more complete evidence supporting the SDH. The credibility of a SDH can be evaluated by

$$Credibility = \alpha_1 \frac{N_{SM.Correct} - N_{SM.Incorrect}}{N_{SM.Correct} + N_{SM.Unreport}} + \alpha_2 \frac{N_{SM.Cluster.Correct}}{N_{SM.Correct}} + \alpha_3 \frac{N_{FI.Correct}}{N_{FI.involve}} \quad (41)$$

where $N_{SM.Correct}$ is the number of smart meters reporting a power outage in outage areas. $N_{SM.Unreport}$ is the number of smart meters in outage areas that do not report a power outage.$N_{SM.Incorrect}$ is the number of smart meters that report power outage outside of outage areas. $N_{SM.Cluster.Correct}$ is the number of smart meters clustered correctly into an outage block among all the smart meters correctly reporting the power outage. $N_{FI.Correct}$ is the number of FIs that correctly report fault currents and their directions. $N_{FI.involve}$ is the number of FIs that are involved in this scenario, which includes all FIs that report the fault current and FIs that should report fault currents but do not. Weighting factors α_1 , α_2 and α_3 are positive numbers that sum to 1. The term with weighting factor α_1 represents the credibility from SM evidence which is defined in [22]. For the extended method in this paper that incorporates DERs, the term with weighting factor α_2 represents the credibility from event timestamp evidence. If a smart meter outage notification belonging to an outage block is incorrectly clustered to another outage block in the second level AOM, this term will be smaller than 1. The term with weighting factor α_3 represents the credibility from FI evidence, which incorporates directional capabilities of FI. The weighting factor of each term can be determined by operator's experience. If the functionality of the corresponding devices is more reliable, a larger weight can be assigned for the associated term. In the future, as outage data and indicators are collected over time, the weighting factors of smart meters and FIs can be enhanced by machine learning methods.

The proposed AOM is designed to handle different locations of smart meters, FIs, and PDs. However, from (41), the existence of smart meters with missing PONs, erroneous PON timestamps, and incorrect FI reports will reduce the credibility of the corresponding outage scenario. Therefore, the installation of smart meters and FIs should be considered as the proposed outage management method is applied.

IV. ADVANCED FEEDER RESTORATION (AFR)

A. First Level Restoration Method

Connecting the outage areas to the utility source by system reconfiguration requires a sequence of switch operations. For some switches, it may take longer to operate due to the traffic condition and safety procedure. The objective of this level is to determine the restoration path δ_{path} which represents the optimal switching sequence of those switches to minimize the duration of restoration process while maximizing the total load served based on availability of the utility source. The optimization can be described by a multi-objective model, i.e., Objectives:

$$Min\ t \quad (42)$$

$$Max \sum_{i \in \Omega_{section}} S_i \quad (43)$$

Subject to

i) $t \geq T_j\ , \forall\ j \in \Omega_{SW}$ (44)

ii) Maintain the radial topology

iii) Operational constraints of voltage magnitude and line capacity with power flow check

The objective (42) and (43) is to find the path with minimum switch operation time and maximum load restored. Constraint (44) indicates that the total time required to reach the final configuration depends on the longest switch operation time. S_i represents the total MVA power of section i.

By implementing the spanning tree search [10], a list of feasible trees to restore the system and their operation time can be determined. Ω_{SW} defines the switches to be operated to form a feasible tree identified. The tree configuration Tr with minimum operation time T_{Tr} gives the optimal path δ_{path}.

In this level, a sequence of configurations of the restoration process is determined. These configurations depend on the availability of utility sources and switch operation constraints.

This article has been accepted for publication in a future issue of this journal, but has not been fully edited. Content may change prior to final publication. Citation information: DOI 10.1109/ACCESS.2021.3103477, IEEE Access

B. Second Level Restoration Method

Based on the restoration path and tree configuration T_r provided in the first level, the second level method is used to determine the operation of DERs and other remote controllable switches to restore critical loads before the utility source is available. T_r determined in the first level is separated into multiple areas by switching devices with synchronization capabilities. Islands are formed by these areas. Based on the availability and controllability of different types of DERs, the restoration process with DERs can be divided into multiple timesteps. In each timestep, the boundary of islands changes by operating switch devices. Critical load will be energized by available DERs in each island. The optimal restoration strategy in each timestep is determined by the mixed integer linear programming (MILP) model in this level.

1) Objective function: The objective of this level is to find the optimal operations to maximize the cumulative MWh load serving capability during the specified restoration period given in the first level. Loads are assigned with a weighting factor to represent their critical level. The objective function for this level is given by

$$max \sum_{t}^{\Gamma} \sum_{m}^{\Omega_{Load}} \sum_{p}^{\Phi} C_m u_m^t P_{m.p}^t \Delta t \tag{45}$$

where Γ represents total time steps of the DER restoration stage. Note that $\Gamma = \frac{T_{Tr}}{\Delta t}$, where T_{Tr} is the longest period for switches to be operated for this restoration path. Δt is the length of timestep which is determined by the enter service period of each DER [4] and switch operation time. Ω_{Load} is the set of loads, and Φ is the set of phases. C_m is the criticality of load m, and $P_{m,p}^t$ is the real power consumption of load m at phase p in the time interval t.

In the following constraints, superscript t represents time interval t, subscript i, h represents DERs or a restored feeder, subscript l, j and k represent areas separated by switch devices.

2) Topology constraints: The topology constraints can be represented by

$$s_{ll}^t = 1, \forall l \in \Omega_{area} \tag{46}$$
$$s_{lj}^t \le s_{lk}^t, j \in \delta_{path.l}(k) \tag{47}$$
$$s_{lj}^t = s_{jl}^t, \forall l, j \in \Omega_{area} \tag{48}$$

where s_{lj}^t is a binary variable. If area l and j are in the same island, it will be 1; otherwise, it will be 0. The symbol $\delta_{path.l}(k)$ represents the set of downstream areas of k when area l is the root of the tree Tr given in the first level AFR where $j, k \in \Omega_{area}$. Constraints (46)-(48) represent that, if area j connects to the root area l to form an island in Tr, area k in between should also be connected to l. Ω_{area} represents the set of areas separated by switching devices with synchronization capabilities in Tr.

3) DER operational constraints: The operation of DERs should meet the requirements of intentional islanding [4]. Depending on their control strategy of the inverters and control capability of the governor and excitation systems, the DERs operational constraints can be represented by

$$\sum_{p\in\Phi} PG_{i.p}^t \le (g_i^t + \mu_i^t + \zeta_i^t) PG_{UP.i}, \forall i \in \Omega_{DER} \tag{49}$$
$$\sum_{p\in\Phi} PG_{i.p}^t \ge (g_i^t + \mu_i^t + \zeta_i^t) PG_{LOW.i}, \forall i \in \Omega_{DER} \tag{50}$$
$$\sum_{p\in\Phi} QG_{i.p}^t \le (g_i^t + \mu_i^t + \zeta_i^t) QG_{UP.i} \; \forall i \in \Omega_{DER} \tag{51}$$
$$\sum_{p\in\Phi} QG_{i.p}^t \ge (g_i^t + \mu_i^t + \zeta_i^t) QG_{LOW.i} \; \forall i \in \Omega_{DER} \tag{52}$$
$$k_{i.f} * \left(\sum_{p\in\Phi} PG_{i.p}^t - PG_{UP.i} \right) + \omega_j^f - \omega_o \le (1 - g_i^t) M \;\; \forall i \in \Omega_{DER.j} \tag{53}$$
$$k_{i.f} * (\sum_{p\in\Phi} PG_{i.p}^t - PG_{UP.i}) + \omega_j^f - \omega_o \ge (g_i^t - 1) M \;\; \forall i \in \Omega_{DER.j} \tag{54}$$
$$k_{i.V} * \left(\sum_{p\in\Phi} QG_{i.p}^t - QG_{UP.i} \right) + V_i^t - V_o \le (1 - g_i^t) M \;\; \forall i \in \Omega_{DER} \tag{55}$$
$$k_{i.V} * \left(\sum_{p\in\Phi} QG_{i.p}^t - QG_{UP.i} \right) + V_i^t - V_o \ge (g_i^t - 1) M \;\; \forall i \in \Omega_{DER} \tag{56}$$
$$-(1 - \mu_i^t) M \le \omega_j^t - \omega_o \le (1 - \mu_i^t) M \; \forall i \in \Omega_{DER.j} \tag{57}$$
$$-(1 - \mu_i^t) M \le V_i^t - V_o \le (1 - \mu_i^t) M \;\; \forall i \in \Omega_{DER} \tag{58}$$
$$g_i^t + \mu_i^t + \alpha_i^t \le 1 \; \forall i \in \Omega_{DER} \tag{59}$$
$$-\left(1 - s_{jk}^t\right) M \le \omega_j^t - \omega_k^t \le \left(1 - s_{jk}^t\right) M \;\; \forall j, k \in \Omega_{area} \tag{60}$$
$$\omega_i^t = \omega_0 - k_{i.f} * (P_{out} - P_{ref}) \tag{61}$$
$$V_i^t = V_0 - k_{i.V} * (Q_{out} - Q_{ref}) \tag{62}$$

where $PG_{i.p}^t$ ($QG_{i.p}^t$) represents the phase p real (reactive) power output of DER i at time interval t. Ω_{DER} represents the set of DERs, while $\Omega_{DER.k}$ represents the set of DERs in area k. ω_j represents the steady state frequency of area j after DERs' primary control in this island. V_i represents the terminal voltage magnitude of DER i. g_i^t, μ_i^t, ζ_i^t represent three control modes of DERs [4]. If g_i^t is 1, DER i is in the droop mode, the frequency and voltage magnitudes are constrained by droop relationships (61)-(62) which are linearized and represented by (53)-(56). If μ_i^t is 1, DER i is in an isochronous mode which is described in (57)-(58) [30]. If ζ_i^t is 1, DER i is in constant PQ mode. Constraints (49)-(52) indicate that, if DER i is connected with the system, its power output should be within the capacity limits. The symbols $PG_{LOW.i}$, $PG_{UP.i}$ ($QG_{LOW.i}$, $QG_{UP.i}$) represent the lower and upper bound of real (reactive) power generation. Constraint (59) is applied to intentional island-capable DERs and black start-capable DERs [4]. This constraint can be modified based on each DER's control capability. It indicates that a DER can

be operated in only one mode in each time interval. Constraint (60) represents that real power is shared among all connected islands.

4) Island restoration constraints: The island restoration is constrained based on DERs and their control capabilities. These constraints can be modeled by

$$\gamma_{droop.ij}^{t} \le s_{kj}^{t}, \forall i \in \Omega_{DER.k} \quad (63)$$

$$\gamma_{droop.ij}^{t} \le g_{i}^{t}, \forall i \in \Omega_{DER} \quad (64)$$

$$\gamma_{droop.ij}^{t} \ge s_{kj}^{t} + g_{i}^{t} - 1, \forall i \in \Omega_{DER.k} \quad (65)$$

$$\gamma_{iso.ij}^{t} \le \sigma_{i}^{t}, \forall i \in \Omega_{DER} \quad (66)$$

$$\gamma_{iso.ij}^{t} \le s_{kj}^{t}, \forall i \in \Omega_{DER.k} \quad (67)$$

$$\gamma_{iso.ij}^{t} \ge s_{kj}^{t} + \sigma_{i}^{t} - 1, \forall i \in \Omega_{DER} \quad (68)$$

$$Er_{j}^{t} \ge \gamma_{droop.ij}^{t}, \forall i \in \Omega_{DER} \quad (69)$$

$$Er_{j}^{t} \ge \gamma_{iso.ij}^{t}, \forall i \in \Omega_{DER} \quad (70)$$

$$Er_{j}^{t} \le \sum_{i \in \Omega_{DER}} \gamma_{droop.ij}^{t} + \sum_{i \in \Omega_{DER}} \gamma_{iso.ij}^{t} \ \forall j \in \Omega_{area} \quad (71)$$

$$\gamma_{droop.ij}^{t} + \sum_{h \in \Omega_{DER}} \gamma_{iso.hj}^{t} \le 1 \ \forall i \in \Omega_{DER}, \forall j \in \Omega_{area} \quad (72)$$

$$\omega_{min} \le \omega_{j}^{t} \le \omega_{max} \ \forall j \in \Omega_{area} \quad (73)$$

By applying *McCormick Envelopes*, $\gamma_{droop.ij}^{t}$ and $\gamma_{iso.ij}^{t}$ are constrained by (63)-(68). The notation $\gamma_{droop.ij}^{t}$ will be 1 if area j is energized by a frequency droop controlled DER i. $\gamma_{iso.ij}^{t}$ will be 1 if area j is energized by a frequency isochronous DER or restored feeder i. In constraints (69)-(71), Er_{j}^{t} is a binary variable. It will be 1 if area j is restored in time interval t. Otherwise, it will be 0. Constraints (69)-(71) represent that the frequency and voltage of a restored area are regulated by at least one energy resource [4]. Constraint (72) indicates that isochronous DERs or a restored feeder can regulate frequency and voltage in an island when only one energy resource in this island is required to do so [4, 30]. Constraint (73) indicates that, the frequency of the islands should be within operation limits after the island is energized. A microgrid controller can be used to regulate the system frequency in an island [31].

5) Feeder operational constraints: The feeder generation is constrained by the transformers and their line capacities.

$$-M(1-\sigma_{i}^{t}) \le PF_{i.p}^{t} - P_{Feeder.i.p}^{t} \le M(1-\sigma_{i}^{t}) \quad (74)$$

$$-M\sigma_{i}^{t} \le QF_{i.p}^{t} \le M\sigma_{i}^{t} \quad (75)$$

$$-M\sigma_{i}^{t} \le PF_{i.p}^{t} \le M\sigma_{i}^{t} \quad (76)$$

$$-M(1-\sigma_{i}^{t}) \le QF_{i.p}^{t} - Q_{Feeder.i.p}^{t} \le M(1-\sigma_{i}^{t}) \quad (77)$$

$$-(1-\sigma_{i}^{t})M \le \omega_{j}^{t} - \omega_{o} \le (1-\sigma_{i}^{t})M \quad (78)$$

$$-(1-\sigma_{i}^{t})M \le V_{i}^{t} - V_{o} \le (1-\sigma_{i}^{t})M \quad (79)$$

$$\left(P_{Feeder.i.p}^{t}\right)^{2} + \left(Q_{Feeder.i.p}^{t}\right)^{2} \le S_{i.p.MAX}^{2} \ \forall i \in \Omega_{Feeder} \ \forall p \in \Omega_{Phase.i} \quad (80)$$

where $PF_{i.p}^{t}$ ($QF_{i.p}^{t}$) is the real (reactive) power output of phase p of substation i in time interval t.The big M method used in constraints (74)-(79) represents that feeder i will provide power when $\sigma_{i}^{t} = 1$. The polyhedral linearization of (80) can be found in [32]. Ω_{Feeder} represents the set of utility feeders. $\Omega_{Phase.i}$ represents the set of phases of feeder i. $S_{i.p.MAX}$ is the maximum feeder capacity for phase p. Constraints (78)-(79) indicate that if the island is restored by the feeder, its frequency and voltage will be controlled to a reference value. If an area is energized by a restored feeder, constraints (66)-(68) and (70)-(72) will also be applied to this feeder generation and the corresponding island.

7) Other constraints: Linearized three-phase unbalanced power flow constraints are adopted [33]. Note that, the first order approximation around the operation point of the voltage magnitude is applied at DERs and feeder nodes. For the branches with switches installed, the big M method is applied [7]. The ramping rates of different types of DERs need to be considered which affect the capacity limits at different timesteps in (49)-(52). Linearized voltage regulator constraints are included [34]. Restoration sequence constraints are given by

$$u_{m}^{t} \le u_{m}^{t+1}, \forall m \in \Omega_{Load}, t \in [1, \Gamma - 1] \quad (81)$$

The restoration algorithm determines the restoration actions. Once a load is restored, service will not be disrupted again.

The restoration actions provided by AFR are validated by computation of the nonlinear, unbalanced distribution power flow. Operation constraints, including node voltages, are checked. If any operation constraint is violated, the corresponding constraints of DERs in (49)-(52) will be modified to adjust their power output to remove the violations.

V. SIMULATION RESULTS

The proposed AOM-AFR is tested on modified IEEE 123-Bus distribution feeder and modified IEEE 8500-Node distribution feeder. Optimization problems are solved by Gurobi solver on MATLAB. Computation is performed on a desktop with I7-8700 core CPU and 32 GB RAM.

Case I: Test Scenario on IEEE 123-Bus System

1). The Test System

As shown in Fig. 5, the modified 123-Bus system has 6 DERs, 6 remotely controlled reclosers, 4 normally open tie switches, and 27 fuses.

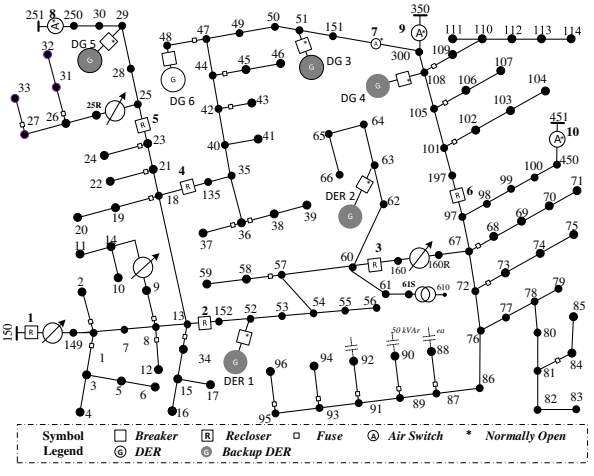

FIGURE 5. Modified IEEE 123-Bus distribution system

This article has been accepted for publication in a future issue of this journal, but has not been fully edited. Content may change prior to final publication. Citation information: DOI 10.1109/ACCESS.2021.3103477, IEEE Access

Each DER is equipped with a circuit breaker with anti-island capability. Among the DERs, DER 1 and DER 2 are batteries with droop-based inverters, while other DERs are diesel generator DGs. DG 6 is connected, normally closed, at node 48. Other DERs are normally open and will provide backup power with the droop control capability.

The capacities and droop characteristics of those droop based DERs are given in Table I.

TABLE I
NORMALLY OPEN DER CHARACTERISTICS

DER Index	Capacity (kW/kVar)	k_f and k_v
DER 1	600/300	$3.33 * 10^{-6}$ and $3.10 * 10^{-5}$
DER 2	900/450	$2.22 * 10^{-6}$ and $2.00 * 10^{-5}$
DG 3	1650/800	$1.21 * 10^{-6}$ and $1.20 * 10^{-5}$
DG 4	900/600	$2.22 * 10^{-6}$ and $1.10 * 10^{-5}$
DG 5	600/210	$3.33 * 10^{-6}$ and $1.18 * 10^{-5}$

To test the integrated AOM-AFR system, a permanent three-phase line-to-ground fault is assumed between node 149 and node 1. Malfunctioning of the PD with DER 6 prolongs its connection. Smart meters in the outage area(s) send outage notifications with timestamps. A FI at R4 indicates the fault current flowing from node 135 to node 18.

A total of 72 hypotheses are tested for AOM. With 15-min timesteps, a 5-step restoration strategy is provided by AFR.

2). Advanced Outage Management (AOM)

A total of 307 smart meters are located at load nodes as shown in Fig. 6.

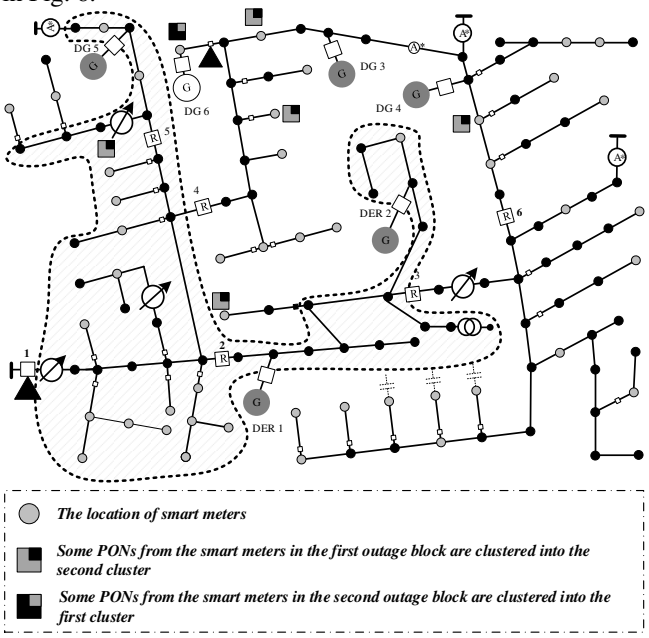

FIGURE 6. Location of smart meters and credible scenarios

Among them, 305 smart meters report the sustained power outage that lasts for more than 45 seconds associated with their event timestamps. For each smart meter that reports the outage, three outage notifications will be sent randomly in 5 seconds. The data will be collected when the first outage notification is received and lasts for 1 minute when the last PON is collected. In this test case, the first outage notification is received 51 second after the occurrence of the fault. The last PON is received in 1 minute and 2 seconds. The total collecting time of these 305 PONs is 1 minute and 11 seconds (one minute threshold plus the period between the time when the first PON is received and time when the last PON is received). Each outage notification contains the timestamp of the outage event.

Based on smart meter outage notifications and FI reports, 72 hypotheses are evaluated. For the hypothesis of 1 fault, 2 outage blocks and 0 FI failure, the boundary of the outage area is determined by the first level AOM of objective (3) with constraints (4)-(5). The actuated PDs and fault location are determined by the second level AOM with K-means clustering algorithm (6), objective (7) and constraints (8)-(40). The fault locations depend on the number of PD miscoordination pairs. In Fig. 6, the actuated recloser and fuse are marked with solid triangles. The most credible location corresponding to 0 or 1 protection mis-coordination pair is the shaded area surrounded by dashed lines. This hypothesis has the highest credibility among all hypotheses based on (41). With 255 correct outage notifications and 12 cluster errors, the credibility of this hypothesis is 0.93 when α_1, α_2, and α_3 values are 0.3, 0.3, and 0.4, respectively. Those cluster errors are indicated in Fig. 6. PONs from 4 smart meters on node 48 in the second outage block are grouped into the first cluster. PONs from 3 smart meters on node 49, 1 smart meter on node 24, 1 smart meter on node 59, and 3 smart meters on node 76 are collected into the second cluster while those smart meters are in the first outage block.

3). Advanced Feeder Restoration (AFR)

The system is separated into 6 areas by switching devices, as shown in Fig. 7. Based on the availability of utility sources and estimated operation times of the manually operated switches in the third column of Table II, the restoration path is determined by the first level AFR.

TABLE II
MANUAL SWITCH OPERATIONAL TIME

Switch	Location (Area)	Estimated Switching Time
SW7	III-VI	75 mins
SW9	node350-VI	60 mins
SW8	node251-II	45 mins
SW10	node451-V	90 mins

With objective (43) and constraints (ii) to (iii), two candidate restoration paths are determined with spanning tree search in [10]. The optimal restoration plan is determined to be SW7, SW8, and SW9 based on objective function (42) and constraint (i), shown by solid triangles in Fig. 7. With the selected restoration path, the restoration strategy is determined by objective function (45) with constraints (46)-(60), (63)-(72), (74)-(79), and (81) with power flow constraints [7, 33, 34]. In this scenario, it is assumed that those DERs have short enter service periods. However, DER 1 and DER 2 can provide energy for no more than 15 minutes due to the capacity limits. All the loads are restored when the area is energized. As shown in Fig. 7, after determining the faulted area the restoration strategy is:

This article has been accepted for publication in a future issue of this journal, but has not been fully edited. Content may change prior to final publication. Citation information: DOI 10.1109/ACCESS.2021.3103477, IEEE Access

$T = 0$ (timestep 0): R2, R4, R5, and R6 are opened. DG4 will connect and serve loads in island VI. DG5 will energize island II. DG3 will energize island III.

$T = 30$ (timestep 2): DER1 will be energized in island IV. The islands IV, V, and VI are synchronized to form a larger island energized by DER1 and DG 4. DG3 will still serve island III, while DG5 will serve island II.

$T = 45$ (timestep 3): SW8 will be closed and island II is restored by the utility source at node 251. DER2 will be synchronized and connected with the system while DER1 is disconnected due to the limited energy availability. The integrated island consisting of IV, V, and VI are energized by DER2 and DG4. DG3 still serves island III.

$T = 60$ (timestep 4): The synchronized islands of IV, V, and VI will be restored by the utility source at node 350 by closing SW9. DG3 continues serving island III.

$T = 75$ (timestep 5): All outage areas are restored by the utility source when SW7 is closed.

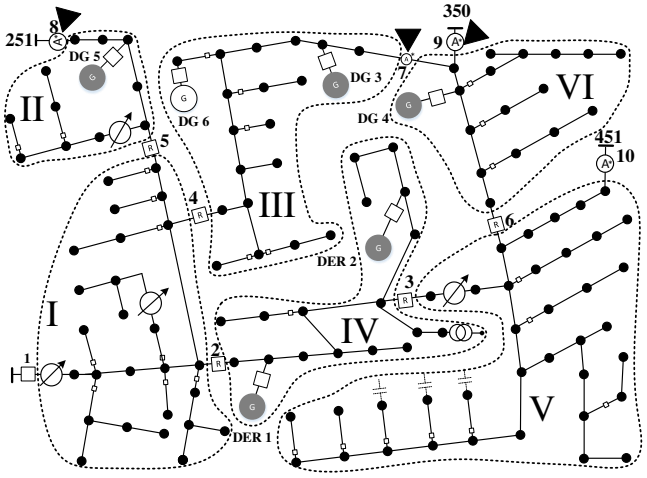

FIGURE 7. Restoration path and switching sequence

4). Comparison with Existing Feeder Restoration Algorithm

AFR is used to find a restoration strategy. To demonstrate the collaboration between the utility source and DERs provided by AFR, DGs and DERs are assumed to have only half of the capacities given in Table I. The outage scenario is the one given in section V (1). The resulting AFR load restoration curve, labeled by *, is shown in Fig. 8.

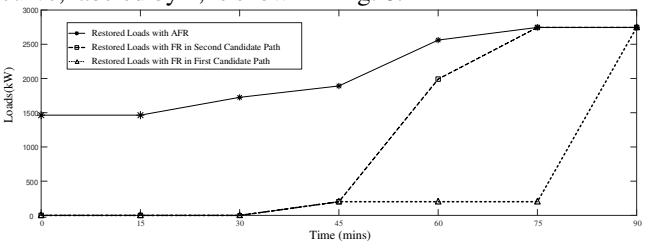

FIGURE 8. Load restoration curves with and without DERs

After isolating the fault by opening R2, R4, and R5, DG3, DG4, and DG5 begin to serve critical loads in the outage area. After 30 minutes, more loads are restored when DER1 is available. At 45 minutes, non-critical loads in island II are restored after closing SW8. DER1 is disconnected and DER2 begins to serve loads in islands III, IV, V, and VI. At 60 minutes, non-critical loads in islands III, IV, V, and VI are restored by closing SW9. Maximum load is restored at 75 minutes when SW7 is closed.

Spanning Tree search reported in [10] has been incorporated in GridLAB-D by Pacific Northwest National Laboratory. In comparison with this feeder restoration (FR) algorithm, the AFR involves multiple DGs and DERs with different characteristics. The availability of DGs and DERs enhances distribution system resilience with respect to extreme events. For the same outage scenario, reclosers R2, R4, and R5 are opened to isolate the fault. For each of these open switches, FR is applied to determine the switch to be closed to maximize the load to be served. Two optimal sets of switching operations are found by FR to restore the maximum load with minimum number of switch operations. The first one is {SW7, SW8, SW10} and the second one is {SW7, SW8, SW9}. Using the same assumption of switch operation times, these two FR strategies result in two load restoration curves, labeled with triangles and squares in Fig. 8.

As shown in Fig. 8, for both switch operation sets from FR, the loads in outage area II in Fig. 7 are restored at 45 minutes when SW8 is closed. For the first operation set, SW7 is closed at 60 minutes. More load is restored when the feeder is picked up by closing switch SW10 at 90 minutes. For the second operation set, loads in outage areas III, IV, V, and VI are restored when the feeder is picked up by closing SW9 at 60 minutes. Maximum load is restored after 75 minutes by closing SW7.

The resilience metric proposed in [1-3, 5] defines resilience as the total weighted MWh energy of critical load served over a given restoration horizon. In this scenario, the restoration horizon is assumed to be 90 minutes, over which restoration actions are completed. The quantified resilience is found by the area under each of the three load restoration curves. The obtained resilience values shown in Table III indicate a significant improvement from FR to AFR due to the availability of multiple DERs and the proposed AOM-AFR strategies.

TABLE IV
RESILIENCE METRIC OF DIFFERENT RESTORATION STRATEGIES

Restoration Strategy	Resilience Achieved (MWh)
First Operation Strategy from FR	2.70
Second Operation Strategy from FR	7.31
AFR Restoration Strategy	19.04

Case II: Test Scenario with IEEE 8500-Node System

As shown in Fig. 9, an IEEE 8500-Node system is modified for validation of the performance of AOM and AFR in a large-scale system. In this modified system, 11 DERs, 21 T class fuses, 5 reclosers, 2 normally opened tie switches, and 18 FIs are included. Among those 18 FIs, 17 have the capability to indicate the direction of fault currents. These two normally open tie switches are assumed to be able to close after 20 minutes. The PD coordination, restoration process, and power flow validation are performed in OpenDSS. Besides the components shown in the figure, loads are assigned to 1177

This article has been accepted for publication in a future issue of this journal, but has not been fully edited. Content may change prior to final publication. Citation information: DOI 10.1109/ACCESS.2021.3103477, IEEE Access

load nodes in the original system. The number of loads in each load node is given by the output of a random integer between 1 and 10 based on a normal distribution. In total, 4732 loads are created, each of them equipped with a smart meter to send the last gasp outage notifications. Loads downstream fuses F4 and F14 are equipped with load control switches (LCS).

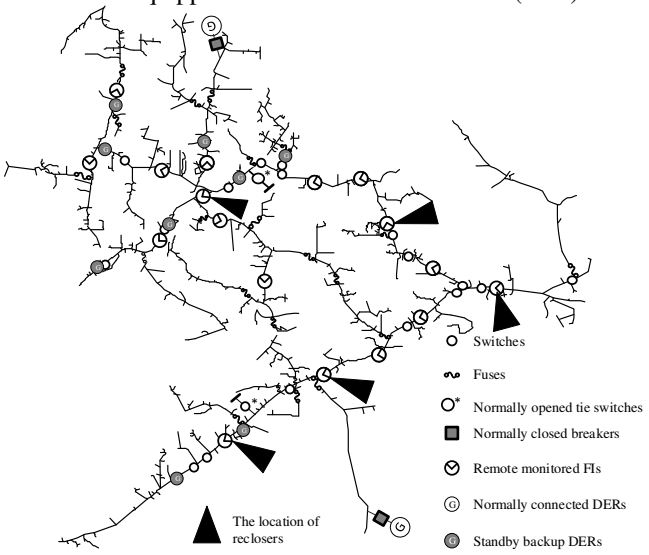

FIGURE 9. **The modified IEEE 8500-node system**

1). Advanced Outage Management (AOM)

The detailed locations of PDs and FIs are shown in Fig. 10.

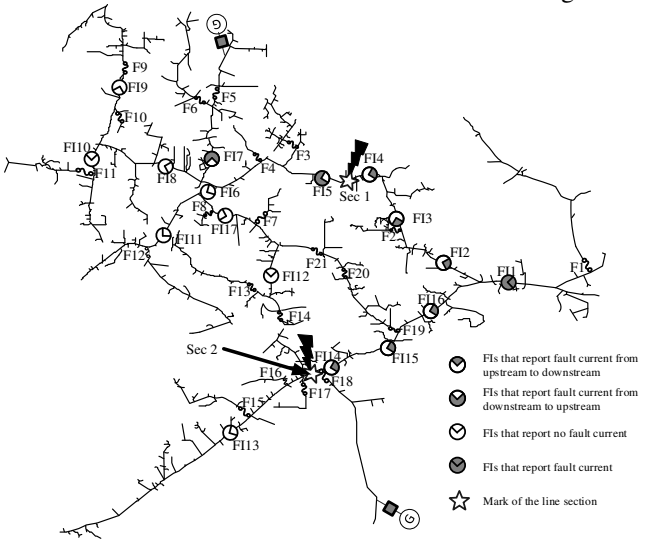

FIGURE 10. **The outage scenario**

The connectors L9407_48332_SW, L5437_48332_SW, V9111_48332_SW, LN4625696_SW, and LN4586093_SW in the original system are modified to be reclosers R1, R2, R3, R4, and R5 where fault indicators FI1, FI3, FI6, FI13, and FI14 are installed, respectively. The outage scenario is simulated by placing two three-phase line-to-ground faults at sections Sec1 and Sec2 marked by stars in Fig. 10 representing LINE.LN6229807-1 and LINE.LN6350529-1 in the original system. The fault locations are indicated by lightning bolts.

Upon the occurrence of these two faults, PDs will be actuated based on their coordination simulated in OpenDSS. The smart meters in the outage area send outage notifications. The FIs report the fault currents. The fault current reports are shown in Fig. 10. 2947 outage notifications with their timestamps are received by AOM.

By applying AOM method to this scenario, two-level hypotheses are generated. By checking 274 hypotheses (calculated in 2mins 40s), the most credible hypotheses set contains 2 faults, 4 outage blocks, and 0 failure of the FIs when α_1, α_2, and α_3 values are 0.3, 0.3, and 0.4, respectively. In the scenario determined by AOM, 2926 PONs are from 3260 smart meters in the outage area. 2230 PONs are correctly clustered by the second level AOM. The credibility for this hypothesis is given by (41) which is 0.896. The possible locations of the first fault are the three-phase sections between FI4 and FI5, and three-phase sections between FI13 and FI14 for the second fault. The blown fuses F5, F18, and actuated reclosers represented by FI3 and FI14 in Fig. 10 are also identified by AOM with this hypothesis. System operators can determine the actual fault locations (Sec1 and Sec2) by checking the set of possible faulted sections identified by AOM.

In comparison with a single-level method, the prior work of the authors [22] is tested with this scenario. With 40 hypotheses tested (maximum 10 faults and three FI failures), the most credible outage scenario has 3 faults with a computation time of 2.47 seconds. The fault locations are the three-phase sections between FI5 and FI6, between FI14 and FI13, and one-phase sections downstream FI7, respectively. In contrast to the proposed AOM in this paper, the method in [22] is not able to identify the correct fault locations in the scenario.

2). Advanced Feeder Restoration (AFR)

The switch devices are modified from connectors in the original system. The locations of DERs and switch devices in this system are illustrated in Fig. 11.

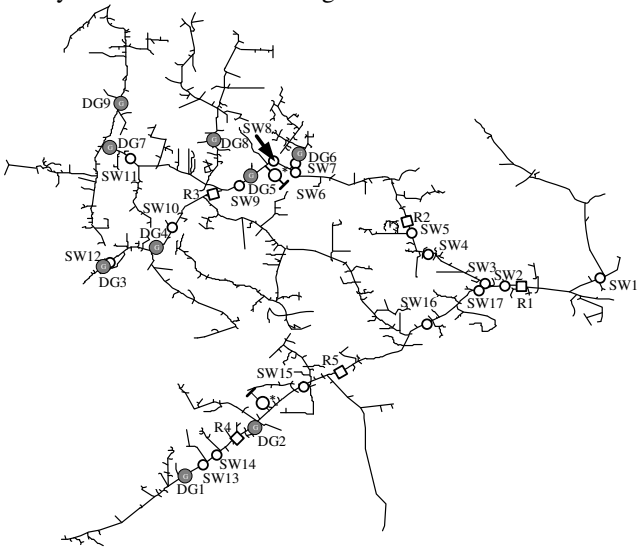

FIGURE 11. **DERs, reclosers and switches**

The faulted sections are isolated by opening R2, SW6 R5, and SW15. As a result, the area downstream of them will be out of utility service for 20 minutes until the normally open tie

This article has been accepted for publication in a future issue of this journal, but has not been fully edited. Content may change prior to final publication. Citation information: DOI 10.1109/ACCESS.2021.3103477, IEEE Access

switches are operated. By applying AFR, the critical loads in the outage areas can be served by DERs in the system which are explained in Table V. The non-critical loads are served as soon as possible when the utility source becomes available.

TABLE V
NORMALLY OPEN DER CHARACTERISTICS

DER Index	Capacity (kW/kVar)	Enter Service Period (min)
DG 1	800/300	4
DG 2	800/300	4
DG 3	700/300	2
DG 4	1000/400	5
DG 5	600/200	1
DG 6	750/200	3
DG 7	600/200	1
DG 8	600/200	1
DG 9	700/200	2

In Fig. 11, these two outage areas are divided into 12 islands by 10 switching devices. With 1-min timesteps, a 20-step restoration strategy of DERs is determined by AFR before normally open tie switches are available (calculated in 2 minutes 12 seconds).

The restoration process is given in Fig. 12. In this figure, the green areas are isolated by open switches due to faults and PD actuations. The red areas are restored by DERs. The blue areas are energized by utility sources. The change of areas in different colors indicates the restoration process in different timesteps. The detailed restoration operations are explained as below:

$\underline{T = 0}$ (timestep 0): R2, SW6 R5, and SW15 will be opened to isolate faults. Fuses F5 and F18 in Fig. 10 are blown due to the fault current contribution from DERs. These switch devices are indicated by yellow triangles in Fig 12 (a).

$\underline{T = 1}$ (timestep 1): When DG5 in Fig. 11 is available, SW9 which is indicated by the purple triangle in Fig. 12 (a) will be opened. Sections between SW9 and SW6 will be energized. The critical loads in the red area will be restored. Although DG7 and DG8 are also available in this timestep, they are not able to connect to the system to form islands.

$\underline{T = 2}$ (timestep 2): When DG3 and DG9 are available, switches SW10 and SW11 indicated by yellow triangles in Fig. 12 (b) are opened. Sections downstream these two switches are energized by DG3. DG7 and DG9. The critical loads in the red areas are restored.

$\underline{T = 3}$ (timestep 3): When DG6 is ready to connect, recloser R3 is opened while SW11 is closed. The switch operations are indicated by yellow triangles in Fig. 12 (c). Sections between R3 and SW6 are energized by DG5, DG6, DG7, DG8 and DG9. The critical loads in the red areas are restored.

$\underline{T = 4}$ (timestep 4): When DG1 and DG2 are ready to serve loads, sections downstream SW15 are energized when DG1, and DG2 are connected. The restored areas after this timestep are shown in red in Fig. 12 (d).

$\underline{T = 5}$ (timestep 5): When DG4 is ready to connect, recloser R3 and switch SW10 are closed which are indicated by yellow triangles in Fig 12 (e). Critical loads in the outage areas are all restored.

$\underline{T = 20}$: When the normally open tie switches are ready to be operated, all loads in the outage area are restored as shown by blue areas in Fig. 12 (f).

This restoration process is validated by the power flow simulation in OpenDSS. This simulation case demonstrates the performance of AOM and AFR in a large-scale distribution system. The AFR method provides the optimal solution using the available energy resources.

The power output changes of DERs and the utility source are indicated in Fig. 13. As shown in the figure, during the period of first 5 minutes, more loads are restored when more DERs are available. Power losses increase due to the expanding restored area. When the utility source is available after 20 minutes, power losses in the area energized by the normally open switches in Fig. 9 are higher compared with the period when those outage areas are restored by 9 DERs.

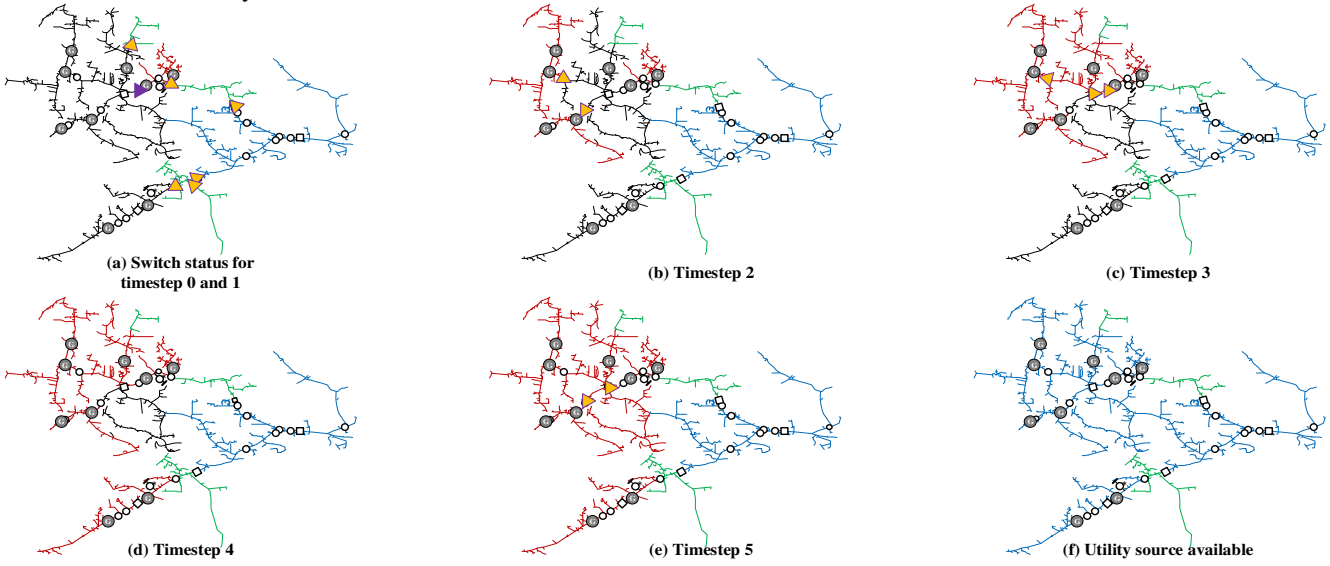

FIGURE 12. The restoration process

This article has been accepted for publication in a future issue of this journal, but has not been fully edited. Content may change prior to final publication. Citation information: DOI 10.1109/ACCESS.2021.3103477, IEEE Access

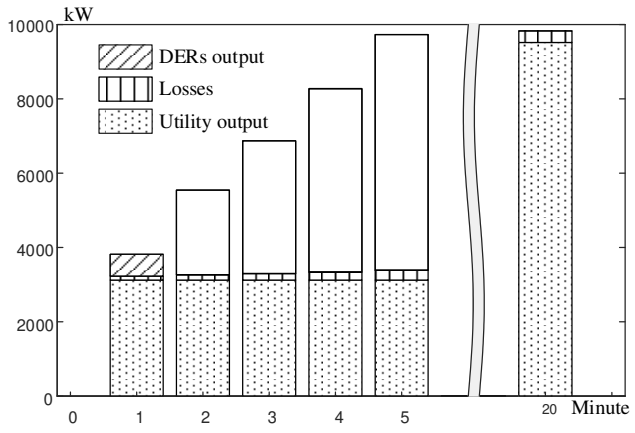

FIGURE 13. Change of power during the restoration process

Case III: Test Scenario with Hazard Condition on IEEE 8500-Node System

To test the performance of AOM under hazard conditions with multiple faults, faults are added to the modified IEEE 8500-node system. In comparison with Case II, three more faults are modified and indicated by lightning bolts in Fig. 14. The PD coordination under this condition is simulated with OpenDSS. A total of 3079 outage notifications with their timestamps are received by AOM.

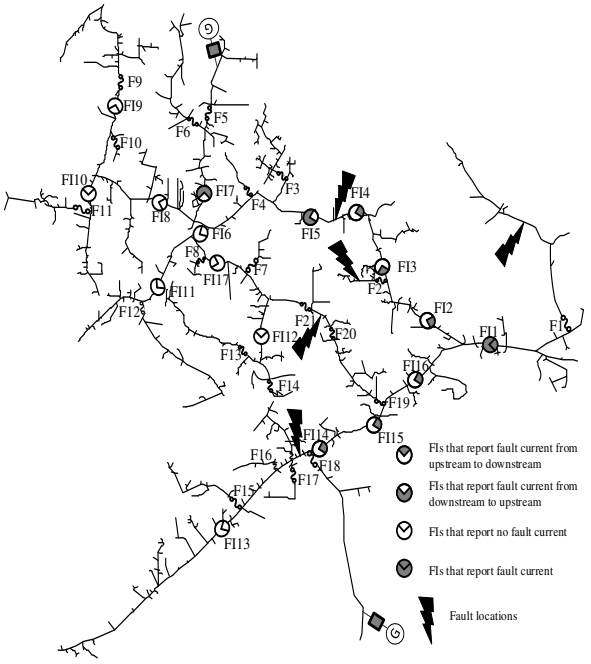

FIGURE 14. Fault locations for Case III

For this given condition and the information received, the most credible outage scenario is identified by evaluating 274 hypotheses in 2 mins and 42s. The most credible set of hypotheses contains 5 faults, 7 outage blocks, and 0 failure of the FIs when α_1, α_2, and α_3 values are 0.3, 0.3, and 0.4, respectively. The possible fault locations are shown in Fig. 15.

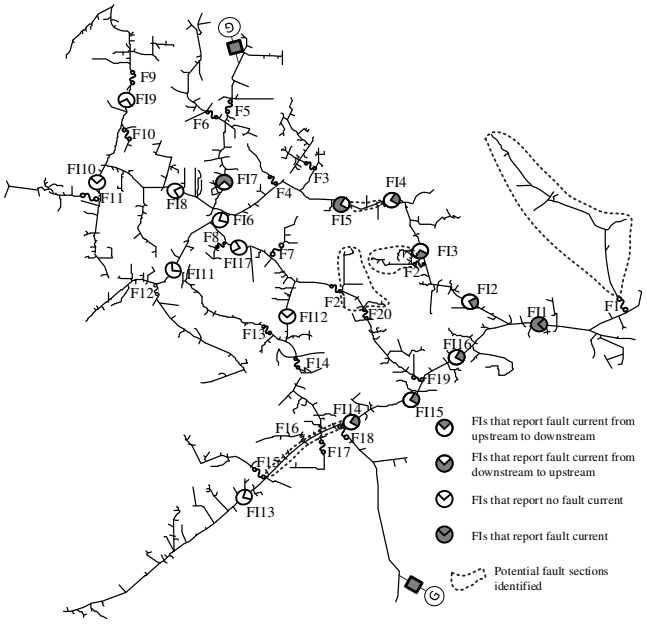

FIGURE 15. Fault locations identified by AOM

The possible location of the first additional fault is identified to be the phase-C sections downstream F1. Three-phase sections downstream F2, and phase-C sections between F20 and F21 are identified to be possible locations of the second and the third additional faults. The blown fuses F1, F2, F5, F18, F20, and actuated reclosers represented by FI3 and FI14 are also identified by AOM under this hypothesis. The list of hypotheses generated in Case II contains the maximum of 20 faults in the system. Therefore, the total calculation time for these two scenarios is almost the same, indicating good performance of the proposed AOM for multiple-fault scenarios.

By comparing Case III with Case II, it is shown that the performance of AOM is not sensitive to the actual number of faults in the system.

VI. CONCLUSIONS

This paper proposes a systematic solution to improve resilience of a system with DERs. The proposed solution is an integrated method with both AOM and AFR. The performance of AOM-AFR method is validated with IEEE test systems.

The AOM determines the outage scenario and actuated PDs based on the available outage evidence from smart meters and FIs. As a hypothesis-based method, the AOM incorporates the incomplete evidence by providing possible outage scenarios associated with a credibility index. In the future, the AOM can be further improved by considering coordination settings of the protection system and the impedance model of the system.

After the outage scenario is determined, the AFR provides the restoration actions to maximize the total MWh of critical loads served after an extreme event. However, the proposed AFR algorithm only considers steady state constraints. In the future work, dynamic constraints and the secondary control in an islanded mode should be incorporated in the methodology.

REFERENCES

[1] Y. Xu, C.-C. Liu, K. P. Schneider, F. K. Tuffner, and D. T. Ton, "Microgrids for Service Restoration to Critical Load in a Resilient Distribution System," *IEEE Trans. Smart Grid*, vol. 9, no. 1, pp. 426–437, Jan. 2018

[2] "Operates Resiliently against Attack and Natural Disaster," U.S. Dept. Energy, Nat. Energy Technol. Lab., Washington, DC, USA, Rep., 2009. [Online]. Available: https://netl.doe.gov/sites/default/files/Smartgrid/Operates-resiliently-against-attack_2009_09_29.pdf

[3] Z. Wang, C. Shen, Y. Xu, F. Liu, X. Wu, and C.-C. Liu, "Risk-Limiting Load Restoration for Resilience Enhancement with Intermittent Energy Resources," *IEEE Trans. Smart Grid*, vol. 10, no. 3, pp. 2507–2522, May 2019

[4] "IEEE Standard for Interconnection and Interoperability of Distributed Energy Resources with Associated Electric Power Systems Interfaces," *IEEE Std 1547-2018 Revis. IEEE Std 1547-2003*, pp. 1–138, Apr. 2018

[5] H. Gao, Y. Chen, Y. Xu, and C.-C. Liu, "Resilience-Oriented Critical Load Restoration Using Microgrids in Distribution Systems," *IEEE Trans. Smart Grid*, vol. 7, no. 6, pp. 2837–2848, Nov. 2016

[6] B. Chen, C. Chen, J. Wang, and K. L. Butler-Purry, "Sequential Service Restoration for Unbalanced Distribution Systems and Microgrids," *IEEE Trans. Power Syst.*, vol. 33, no. 2, pp. 1507–1520, Mar. 2018

[7] Z. Wang, J. Wang, and C. Chen, "A Three-Phase Microgrid Restoration Model Considering Unbalanced Operation of Distributed Generation," *IEEE Trans. Smart Grid*, vol. 9, no. 4, pp. 3594–3604, Jul. 2018

[8] J. Liu, C. Qin and Y. Yu, "A Comprehensive Resilience-Oriented FLISR Method for Distribution Systems," *IEEE Trans. Smart Grid*, Dec. 2020

[9] J. C. Bedoya, J. Xie, Y. Wang, X. Zhang, and C.-C. Liu, "Resiliency of Distribution Systems Incorporating Asynchronous Information for System Restoration," *IEEE Access*, vol. 7, pp. 101471–101482, 2019

[10] J. Li, X.-Y. Ma, C.-C. Liu, and K. P. Schneider, "Distribution System Restoration with Microgrids Using Spanning Tree Search," *IEEE Trans. Power Syst.*, vol. 29, no. 6, pp. 3021–3029, Nov. 2014

[11] A. Abel Hafez, W. A. Omran, and Y. G. Hegazy, "A Decentralized Technique for Autonomous Service Restoration in Active Radial Distribution Networks," *IEEE Trans. Smart Grid*, vol. 9, no. 3, pp. 1911–1919, May 2018

[12] W.-H. Chen, "Quantitative Decision-Making Model for Distribution System Restoration," *IEEE Trans. Power Syst.*, vol. 25, no. 1, pp. 313–321, Feb. 2010

[13] S. Yao, P. Wang, X. Liu, H. Zhang, and T. Zhao, "Rolling Optimization of Mobile Energy Storage Fleets for Resilient Service Restoration," *IEEE Trans. Smart Grid*, vol. 11, no. 2, pp. 1030-1043, March 2020

[14] J. Northcote-Green and R. Wilson, *Control and Automation of Electrical Power Distribution Systems*, 1st ed. CRC Press, 2017.

[15] S. Chaitusaney and A. Yokoyama, "Prevention of Reliability Degradation from Recloser–Fuse Miscoordination due to Distributed Generation," *IEEE Trans. Power Deliv.*, vol. 23, no. 4, pp. 2545–2554, Oct. 2008

[16] A. F. Naiem, Y. Hegazy, A. Y. Abdelaziz, and M. A. Elsharkawy, "A Classification Technique for Recloser-Fuse Coordination in Distribution Systems with Distributed Generation," *IEEE Trans. Power Deliv.*, vol. 27, no. 1, pp. 176–185, Jan. 2012

[17] S. T. Mak, "A Synergistic Approach to Using AMR and Intelligent Electronic Devices to Determine Outages in a Distribution Network," in *2006 Power Systems Conference: Advanced Metering, Protection, Control, Communication, and Distributed Resources*, Mar. 2006

[18] R. Fischer, A. Laakonen, and N. Schulz, "A General Polling Algorithm Using a Wireless AMR System for Restoration Confirmation," *IEEE Power Eng. Rev.*, vol. 21, no. 4, pp. 70–70, Apr. 2001

[19] M. Kezunovic, "Smart Fault Location for Smart Grids," *IEEE Trans. Smart Grid*, vol. 2, no. 1, pp. 11–22, Mar. 2011

[20] J.-H. Teng, W.-H. Huang, and S.-W. Luan, "Automatic and Fast Faulted Line-Section Location Method for Distribution Systems Based on Fault Indicators," *IEEE Trans. Power Syst.*, vol. 29, no. 4, pp. 1653–1662, Jul. 2014

[21] Y. Jiang, "Data-Driven Fault Location of Electric Power Distribution Systems with Distributed Generation," *IEEE Trans. Smart Grid*, vol. 11, no. 1, pp. 129-137, Jan. 2020

[22] Y. Jiang, C.-C. Liu, M. Diedesch, E. Lee, and A. K. Srivastava, "Outage Management of Distribution Systems Incorporating Information from Smart Meters," *IEEE Trans. Power Syst.*, vol. 31, no. 5, pp. 4144–4154, Sep. 2016

[23] I. Džafić, R. A. Jabr, S. Henselmeyer, and T. Đonlagić, "Fault Location in Distribution Networks through Graph Marking," *IEEE Trans. Smart Grid*, vol. 9, no. 2, pp. 1345–1353, Mar. 2018

[24] F. C. L. Trindade and W. Freitas, "Low Voltage Zones to Support Fault Location in Distribution Systems with Smart Meters," *IEEE Trans. Smart Grid*, vol. 8, no. 6, pp. 2765–2774, Nov. 2017

[25] S. Chakraborty and S. Das, "Application of Smart Meters in High Impedance Fault Detection on Distribution Systems," *IEEE Trans. Smart Grid*, vol. 10, no. 3, pp. 3465-3473, May 2019

[26] K. Samarakoon, J. Wu, J. Ekanayake, and N. Jenkins, "Use of Delayed Smart Meter Measurements for Distribution State Estimation," *2011 IEEE Power and Energy Society General Meeting*, Detroit, MI, USA, 2011, pp. 1-6

[27] Introduction of Centron https://www.itron.com/-/media/feature/products/documents/spec-sheet/centron-gprs-smartmeter.pdf

[28] C. Chen, J. Wang, and D. Ton, "Modernizing Distribution System Restoration to Achieve Grid Resiliency Against Extreme Weather Events: An Integrated Solution," *Proceedings of the IEEE*, vol. 105, no. 7, pp. 1267-1288, July 2017

[29] G. P. McCormick, "Computability of Global Solutions to Factorable Nonconvex Programs: Part I — Convex Underestimating Problems," *Math. Program.*, vol. 10, no. 1, pp. 147–175, Dec. 1976

[30] K. Prabha, "Power System Stability and Control," Vol. 7. New York: McGraw-Hill, Inc, 1994, pp. 581-617

[31] "IEEE Standard for the Specification of Microgrid Controllers," *IEEE Std 20307-2017*, pp. 1–43, Apr. 2018

[32] A. Ben-Tal and A. Nemirovski, "On Polyhedral Approximations of the Second-Order Cone," Math. Oper. Res., vol. 26, no. 2, pp. 193–205, May 2001

[33] L. Gan and S. H. Low, "Convex Relaxations and Linear Approximation for Optimal Power Flow in Multiphase Radial Networks," in *2014 Power Systems Computation Conference*, Aug. 2014, pp. 1–9

[34] W. Wu, Z. Tian, and B. Zhang, "An Exact Linearization Method for OLTC of Transformer in Branch Flow Model," *IEEE Trans. Power Syst.*, vol. 32, no. 3, pp. 2475–2476, May 2017

Chensen Qi (SM'20) received the B.E. degree in electrical engineering and automation from Zhejiang University, Hangzhou, China, in 2016. He is currently pursuing his Ph.D. degree at Power and Energy Center, Virginia Tech.

Chen-Ching Liu (F'94, LF'19) is currently American Electric Power Professor and Director of Power and Energy Center, Virginia Tech. He is also an Adjunct Full Professor of University College Dublin, Ireland. Dr. Liu is a Member of the U.S. National Academy of Engineering.